Title
The Effects of Canopy Morphology on Flow Over a Two-Dimensional Isolated Ridge

Journal
Journal of Geophysical Research: Atmospheres, 125(19)

ISSN
2169-897X

Authors
Ma, Yulong
Liu, Heping
Banerjee, Tirtha
et al.

Publication Date
2020-10-16

DOI
10.1029/2020jd033027

Peer reviewed

JGR Atmospheres

RESEARCH ARTICLE
10.1029/2020JD033027

The Effects of Canopy Morphology on Flow Over a Two-Dimensional Isolated Ridge

Yulong Ma[1], Heping Liu[1], Tirtha Banerjee[2], Gabriel G. Katul[3], Chuixiang Yi[4], and Eric R. Pardyjak[5]

[1]Department of Civil and Environmental Engineering, Washington State University, Pullman, WA, USA, [2]Department of Civil and Environmental Engineering, University of California, Irvine, CA, USA, [3]Nicholas School of the Environment and Department of Civil and Environmental Engineering, Duke University, Durham, NC, USA, [4]School of Earth and Environmental Sciences, Queens College, City University of New York, New York, NY, USA, [5]Department of Mechanical Engineering, University of Utah, Salt Lake City, UT, USA

Key Points:
- Flows over the leeward side of a partially and fully forested hill are studied using a multiple-layer canopy module in the WRF-LES
- Canopy morphologies and partial forest cover lead to pressure perturbations that deviate from hydrostatic approximation
- The leeward recirculation is altered by canopy morphological changes and partly modulated the pressure-velocity interaction

Supporting Information:
- Supporting Information S1

Correspondence to:
H. Liu,
heping.liu@wsu.edu

Citation:
Ma, Y., Liu, H., Banerjee, T., Katul, G. G., Yi, C., & Pardyjak, E. R. (2020). The effects of canopy morphology on flow over a two-dimensional isolated ridge. *Journal of Geophysical Research: Atmospheres*, *125*, e2020JD033027. https://doi.org/10.1029/2020JD033027

Received 1 MAY 2020
Accepted 30 AUG 2020
Accepted article online 2 SEP 2020

Abstract Momentum and mass exchanges between the atmosphere and forests situated on complex terrain continue to draw significant research attention primarily because of their significance to a plethora of applications. In this paper, we investigated flows behavior on the leeward side of a two-dimensional forested ridge under neutrally stratified conditions using large-eddy simulations (LESs). The goal is to understand how variations in leaf area index (LAI), vertical canopy foliage distributions, and forest edge positions affect mean/turbulent flow statistics, momentum fluxes, and onset of recirculation patterns. Although pressure perturbations are dominated by the hill shape, it is demonstrated here that changes in canopy foliage distribution modulate intensities and patterns of the leeward adverse pressure gradients. Such changes in the adverse pressure gradients alter the mean velocity streamlines including the patterns and magnitudes of the leeward downward mean vertical velocity and the velocity variances and momentum flux in the wake region. While a downwind recirculation zone develops in all cases, the details regarding the incipient location and recirculation zone size vary including positions of the separation and reattachment points. Furthermore, changes in the strength and depth of the zone occur due to canopy-induced changes in adverse pressure gradients, advection, and canopy drag. Because the recirculation zone impacts the local mean advective terms in momentum and scalar exchanges, the simulations here indicate that canopy morphology-induced changes in the leeward flows have significant implications to both measurements and models of biosphere-atmosphere exchange over complex terrain.

1. Introduction

Flows over the leeward side of a hill are characterized by a strong elevated shear layer and a highly turbulent wake region. They have received a great deal of attention in many applications such as eddy covariance flux measurements, forest fire controls, wind turbine sitting, and forest management in hilly terrain (e.g., Kutter et al., 2017; Simpson et al., 2013; Yang et al., 2015; Zitouna-Chebbi et al., 2015). Canopy flows over hills covered by vegetation have been studied using wind-tunnel (Finnigan & Brunet, 1995) and flume experiments (Poggi & Katul, 2007a, 2007b, 2007c), field measurements (Morse et al., 2002), analytical models (Finnigan & Belcher, 2004; Harman & Finnigan, 2010; Poggi et al., 2008; Wang & Yi, 2012), closure models (Bitsuamlak et al., 2004; Finnigan et al., 2015; Grant et al., 2016; Katul et al., 2006; Katul & Poggi, 2010; Kobayashi et al., 1994; Ross, 2011; Wilson et al., 1998), and over the past decade or so by large-eddy simulations (LESs) (B. Chen et al., 2019; Dupont et al., 2008; Patton & Katul, 2009; Ross, 2008). Compared to flow over gentle hills where the roughness is characterized by a single momentum roughness height value (e.g., Allen, 2006; Belcher & Hunt, 1998; Cao et al., 2012; H. Chen & Yi, 2012; Liu et al., 2016, 2019; Pearse et al., 1981), the presence of porous tall forest canopies introduces new features on the leeward side such as within canopy mean recirculation.

It is known that the combined effect of the canopy-hill system on flows is largely associated with topography and canopy length scales (Poggi et al., 2008; Ross & Vosper, 2005). For stationary conditions, the balance in the mean momentum transport includes mean advection, mean pressure gradients, turbulent stress gradients, and canopy drag from elements. On the leeward side of the hill and deep within the canopy, the turbulent stress and its gradient may be small resulting in a dominant balance between drag force,

advection, and adverse pressure gradient. This balance was shown to lead to a region of negative longitudinal velocity within the canopy consistent with a mean recirculation pattern (Finnigan & Belcher, 2004; Poggi et al., 2008). This recirculation zone mainly develops on the leeward side of a hill (adverse mean pressure gradient) with sufficiently tall and dense canopy so as to absorb all the momentum flux within the canopy volume (B. Chen et al., 2019; Finnigan & Belcher, 2004; Harman & Finnigan, 2010; Patton & Katul, 2009; Poggi et al., 2008; Ross & Vosper, 2005; Xu & Yi, 2013). After considering the impact of canopy density with uniformly distributed foliage on flows over hills, Patton and Katul (2009) showed that an increase in the canopy density promotes a leeward flow separation within the canopy. Densely arrayed canopy elements reduce the so-called adjustment length scale and the mixing length associated with momentum exchange, which tend to promote such recirculation zone development (Banerjee et al., 2013; Belcher et al., 2008, 2012; Finnigan & Belcher, 2004; Kröniger et al., 2018). However, canopy drag reduces the flow speed within canopy layers (Dupont & Brunet, 2008; Shaw & Patton, 2003; Yi, 2008), which reduces the strength of the recirculating flow (Belcher et al., 2012). In addition, the leeward recirculation is a highly intermittent region rather than a stable vortex (or "rotor-like" motion) as illustrated by flow visualization in flume experiments (Poggi & Katul, 2007a, 2007b, 2007c). The impact of near-surface recirculation induced by different surface conditions on turbulence appears mainly restricted within the canopy (Patton & Katul, 2009; Poggi & Katul, 2008) even as the hill slope steepens (B. Chen et al., 2019).

Moving from the mean flow to turbulent quantities, highly covariant turbulent structures are generated near the canopy top at the summit and then advected further downwind in the wake region where turbulence further develops and interacts with the canopy downwind of the hill (Dupont et al., 2008; Ross, 2008). LES results over a forested hill suggest that turbulence in the wake region is associated with interactions of large turbulence structures generated by the elevated shear layer that may result from the rolling over of Kelvin-Helmholtz (KH) instabilities, structures induced by an adverse pressure gradient at the leeward foot of the hill, and canopy-induced structures (Dupont et al., 2008). Surprisingly, flume experiments and LES results suggest that for dense canopies, second-order flow statistics inside canopies still scale with the local friction velocity formed at the canopy top and the canopy height (B. Chen et al., 2019). This collapse in data using local friction velocity invites the usage of the so-called moving equilibrium hypothesis proposed in the late 1970s (Kader & Yaglom, 1978; Yaglom, 1979). Conditional analysis of LES results and flume experiments also demonstrates that momentum transport within forested canopies on the leeward of a hill is still dominated by sweeps (Poggi & Katul, 2007a) similar to those found within canopies over flat terrain (Poggi et al., 2004; Ross, 2008).

A variety of natural and anthropogenic disturbances (e.g., forest fire and logging) generate heterogeneous forested landscapes with edges over hills. These edges do generate an extra disturbance that modifies the canonical picture of uniform canopy flow covering two-dimensional ridges. It was found that the recirculation flow patterns are sensitive to the locations of forest edges over a forested hill with a gentle slope covered with uniform canopy densities (Ross & Baker, 2013). However, for gentle slopes (e.g., $H/L < 0.1$, where H is the hill height and L is the hill half-length), it is expected that forest edges play a more dominant role compared to the slope-induced effects in influencing flow separation and recirculation. The canopy edge-induced pressure gradient can be locally larger than the hill-induced pressure gradient, depending on the position of the forest edge relative to the hill. However, the influence of the edge-induced pressure gradient is primarily localized to the vicinity of the canopy edge and some downstream distance thereafter (Banerjee et al., 2013; Cassiani et al., 2008; Fontan et al., 2013; Ross & Baker, 2013). What remains relatively less explored is how the variations in canopy morphology (restricted here to foliage amount as measured by leaf area index or LAI and vertical foliage area per unit volume distribution or leaf area density, LAD) and forest edge positions (i.e., forest to clearing transition on the leeward side) modulate turbulence structures and recirculation features over a hill with a moderate slope, which motivates this study. A moderate slope of $H/L = 0.3$ is chosen here such that the effects of both the hill slope and canopy morphology are both dynamically important.

The objectives are thus to explore (1) the influence of varying canopy foliage distribution and (2) the influence of varying forest edge positions in the leeward side of a hill on the flow statistics. Seven LES cases are designed with different canopy foliage amount and distribution and forest edge positions, aiming to unpack the interplay of topography, canopy morphologies, and canopy heterogeneity on mean and turbulent flow in general and the recirculation zone in particular. Section 2 describes the numerical model used and the setup

of the simulations for the seven cases. Section 3.1 discusses the effects of changes in LAD on the leeward recirculation, which is followed by section 3.2 in which the effects of changes in vertical foliage distribution on the leeward flow are then studied. Section 3.3 presents the effects of changing canopy edge position on the leeward flow. Finally, section 4 provides conclusions.

2. Numerical Method

2.1. Model Description

The Weather Research and Forecasting model with the large-eddy simulation module (WRF-LES, Skamarock et al., 2008) is employed. In the WRF-LES model, large energetic eddies are explicitly resolved but small eddies are parameterized using a subgrid-scale (SGS) scheme. The WRF-LES model integrates the instantaneous and filtered momentum conservation equation given by

$$\frac{\partial \overline{u}_i}{\partial t} + \partial \overline{u}_i\, \overline{u}_j \over \partial x_j = -\frac{1}{\rho}\frac{\partial \overline{p}}{\partial x_i} - \frac{\partial \tau_{ij}}{\partial x_j} + F_{u,\,i}, \tag{1}$$

where t is time, $\overline{u}_i$ is the filtered velocity in the i direction x_i with $i = 1$, 2, and 3 corresponding to a rectilinear system with streamwise (x), spanwise (y), and vertical (z) directions, respectively, ρ is the mean air density (density fluctuations are not considered by design), $\overline{p}$ is the filtered pressure, τ_{ij} represents the SGS stresses that are parameterized using a SGS scheme, and $F_{u,i}$ is an external drag force to represent the effects of the vegetation on the resolved flow. The scale-dependent Lagrangian dynamic model (Bou-Zeid et al., 2005) is adopted here to parameterize the SGS stresses, which shows promising performance in predicting turbulence over complex terrain as discussed elsewhere (Ma & Liu, 2017).

The aforementioned aerodynamic drag by canopy elements is modeled using a porous body assumption, with the drag force being expressed as

$$F_{u,\,i} = -c_d a |U| \overline{u}_i, \tag{2}$$

where c_d is the drag coefficient set to a constant 0.2 as discussed elsewhere (Katul et al., 2004), $a(z)$ is the LAD for each canopy layer, and U is the local wind speed. The constant c_d may be questionable because it ignores any Reynolds number dependencies that can occur in the deeper layers of the canopy, as well as sheltering and blockage as discussed elsewhere (Wang et al., 2019). Nonetheless, what is relevant is the product of $c_d a$, and variations in $a(z)$ or its vertically integrated value (=LAI) can often exceed any adjustments to c_d. Moreover, a number of closure models and LES runs have shown that measured higher-order turbulence statistics can be reasonably reproduced within forested canopies even when setting c_d to a constant (B. Chen et al., 2019; Juang et al., 2008; Katul & Chang, 1999; Lin et al., 2018; Massman, 1997; Meyers, 1986; Wilson, 1988; Wilson & Shaw, 1977;). This parameterization of the canopy drag force is a submodule in an advanced multiple-layer canopy module (MCANOPY), which takes into account all important physical and physiological canopy processes within a forest canopy and is coupled with the WRF-LES model (Ma & Liu, 2019). The MCANOPY module was evaluated and then used to simulate forest edge flows reported elsewhere (Ma et al., 2020).

2.2. Simulation Configurations

All simulations are performed in a rectangular domain of 1.2 km × 0.36 km × 0.25 km in the x, y, and z directions, respectively. The horizontal grid resolution is 3 m, and the vertical resolution is 1 m within the canopy and stretched above to a 5-m grid spacing at the domain top. With these configurations, the number of grid nodes in the (x, y, and z) directions is (400, 120, and 65). At the top of the domain, a rigid boundary is used by setting the vertical velocity to 0, and a free-slip boundary is used for horizontal velocities and stresses. A Rayleigh damping layer on the vertical velocity is applied at the top 10% of the domain height to prevent reflection of gravity waves. To ensure prevailing winds along the x direction, Coriolis effects are ignored and a constant pressure gradient is externally imposed along the streamwise direction to drive the flow, similar to that in Patton and Katul (2009). Our tests show that including the Coriolis term introduces a minor impact on the flow features due to the small-scale hill and the neutral atmospheric stability in line with

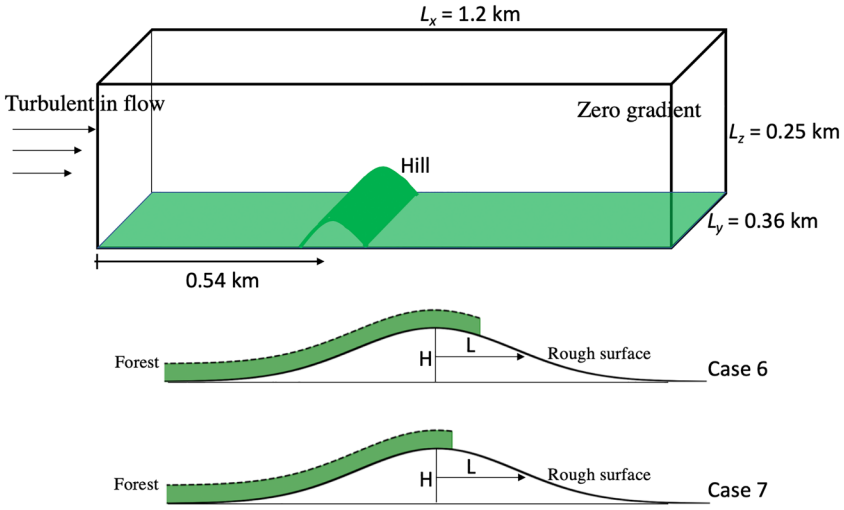

Figure 1. Sketch of the domain. *Lx*, *Ly*, and *Lz* are the domain length, width, and height, respectively. The ridge height is $H = 30$ m, and its half-width is $L = 100$ m. The momentum roughness length for the cleared ground in Cases 6 and 7 is taken as 0.1 m.

prior findings by Belcher and Hunt (1998). A turbulent inflow at the western lateral boundary is provided to keep the same inflow conditions for all LES runs. This inflow field is generated from a precursor simulation in which the domain size and grid resolutions are the same as those in the real runs but with the periodic boundary conditions over flat terrain previously used in Ma and Liu (2017). The northern and southern boundaries are set periodic. The chosen resolution and boundary conditions have been used for studying the flow features over highly complex terrain (Ma & Liu, 2017) and flow dynamics and scalar transport near a forest edge (Ma et al., 2020).

As illustrated in Figure 1, a two-dimensional hill is placed in the domain with the summit located 0.54 km from the upwind boundary of the domain. With the turbulent inflow condition at the western boundary and the zero-gradient boundary at the east, the hill can be considered totally isolated. The height for the two-dimensional hill with a moderate slope considered here is described by the hill function $z_{hill}/H = \exp\left[-\left(\frac{x}{L}\right)^2\right]$, where $H = 30$ m is the hill peak height and $L = 100$ m is the half-width of the hill base. The canopy height h is set as 10 m with a vertically uniformly distributed LAI of 3 m^2 m^{-2} unless stated otherwise (see Table 1) yielding a canopy LAD $a = LAI/h$ and an adjustment length scale $L_c = (C_d a)^{-1} = 16.7$ m, with C_d being a constant value of 0.2. Based on the linearized theory in Finnigan and Belcher (2004), these numerical configurations result in the middle layer height $h_m = 47.8$ m ($h_m/H = 1.59$) and the inner layer height $h_i = 11.0$ m ($h_i/H = 0.37$). All seven simulations are performed under neutral stability conditions.

The model is run for 50 min with the first 20 min being the spin-up time. The data in the following 30 min, corresponding to approximately 5.5 times the eddy turnover time, with the output time interval of 1 s are used in the analysis. The mean quantities are computed from a space- (y direction) and time-averaging procedure, denoted by the symbol $\langle\ \rangle$. The turbulence fluctuations are defined as the departures from the mean values at each height, denoted by the symbol prime ($'$).

3. Results and Discussion

Three cases with the uniformly distributed foliage but different LAI values are explored first, followed by two cases with the same LAI but different vertical foliage distributions and then by two cases with the uniform foliage distribution and the same LAI but with different forest coverage regions longitudinally (Table 1). Since the flow patterns upwind of the hill remain unchanged for all cases, the focus is on leeward flows.

The first- and second-order moments of the flow to be analyzed include normalized mean streamwise velocity $\frac{\langle U \rangle}{\langle U_{\mathrm{ref}} \rangle}$, normalized streamwise velocity variance $\frac{\langle u'u' \rangle}{\langle U_{\mathrm{ref}}{}^2 \rangle}$, normalized spanwise velocity variance $\frac{\langle v'v' \rangle}{\langle U_{\mathrm{ref}}{}^2 \rangle}$,

Table 1
Parameters Characterizing the Flows for Each LES Case

Name	Forest coverage	LAI ($m^2\ m^{-2}$)	Foliage distribution	Separation point[a] (x/H)	Reattachment point (x/H)
Case 1	Fully	1.5	Uniform	1.4	8.8
Case 2	Fully	3.0	Uniform	1.0	9.8
Case 3	Fully	6.0	Uniform	0.8	13.5
Case 4	Fully	3.0	Sparse in lower layers	2.2	12.0
Case 5	Fully	3.0	Dense in lower layers	1.0	9.2
Case 6	$x/H < 1.9$	3.0	Uniform	1.0	6.3
Case 7	$x/H < 0.5$	3.0	Uniform	0.9	5.7

[a]The separation point and reattachment point are determined from the mean streamwise velocity field where the mean streamwise velocity becomes 0 at the surface. The summit is located at $x/H = 0$. Cases 6 and 7 are for partially covered forested hill. The downwind forest edge is terminated at a preset x/H.

normalized vertical velocity variance $\frac{\langle w'w' \rangle}{\langle U_{\mathrm{ref}}{}^2 \rangle}$, and normalized momentum flux $\frac{\langle u'w' \rangle}{\langle U_{\mathrm{ref}}{}^2 \rangle}$, where $\langle U_{\mathrm{ref}} \rangle$ is defined as the mean velocity at the height of 6 h far upwind of the hill (i.e., a location over a flat terrain at $x/H = -15$). All second-order statistics are calculated by the resolved components.

The results to be discussed focus on the recirculation zone inferred from the mean momentum balance (i.e., zones with negative longitudinal velocity), which is given by

$$\underbrace{\left(< U > \frac{\partial < U >}{\partial x} + < W > \frac{\partial < U >}{\partial z} \right)}_{Advection} = \underbrace{-\frac{1}{< \rho >} \frac{\partial < P >}{\partial x}}_{Pressure\ Gradient} \underbrace{- \left(\frac{\partial < u'w' >}{\partial z} + \frac{\partial < u'u' >}{\partial x} \right)}_{Turbulent\ Stresses} \underbrace{- \frac{< |U| > < U >}{Lc}}_{Drag\ Force}, \quad (3)$$

where the flow is assumed to be stationary (by design) and high Reynolds number so that the viscous stresses are ignored. The mean pressure gradient is impacted by the hill shape (e.g., a hydrostatic approximation) and interactive effects between the velocity (mean and turbulent) and the pressure (expected from the Poisson equation for the pressure). The simplest case leading to a recirculation can be expected in the deeper layers of a tall and dense canopy where the mean advection term and turbulent stress divergence terms are small, with the drag force the only term balancing the adverse pressure gradient (expected on the leeward). Runs 1 to 7 are intended to explore how canopy morphology impacts this simplified picture. Also, when the turbulent stress divergence is small but advection remains significant, the flow may be labeled as "turbulently inviscid" (e.g., Banerjee et al., 2013) because only mean flow quantities impact the character of the solution for $\langle U \rangle$ and $\langle W \rangle$.

3.1. Influence of LAI on the Leeward Flow

The analysis is based on Case 1 (LAI = 1.5 $m^2\ m^{-2}$), Case 2 (LAI = 3 $m^2\ m^{-2}$), and Case 3 (LAI = 6 $m^2\ m^{-2}$), and all these three cases have uniformly distributed foliage (Table 1) with a = LAI/h. In general, the major features of mean and turbulent flows over the fully forested hill in all three cases are consistent with prior findings (e.g., Belcher et al., 2012; Dupont et al., 2008; Patton & Katul, 2009) and are not repeated here (supporting information Figures S1–S6). Therefore, the focus is on leeward flow changes resulting from changes in canopy morphologies.

3.1.1. Changes in Recirculation

It is expected that the separation point is at the location (e.g., taking Case 1 with $x/H = 1.5$ as an example here) where the hill-induced pressure gradient (+), horizontal advection (+), vertical momentum transferred into the canopy (+), and canopy drag (−) when $x/H < 1.4$ are balanced by the hill-induced adverse pressure gradient force (−), vertical momentum transferred into the canopy (+), and canopy drag (+) when $x/H > 1.5$. Here, the positive sign is defined as the force acts toward the positive x/H (Figure 2). Clearly, the separation point moves toward the summit and the reattachment point reaches farther downstream (Figure 2 and Table 1), leading to an enlarged recirculation as LAI increases from Case 1 to Case 2 and to Case 3. For extreme cases with very dense, vertically uniformly distributed canopies with LAI > 10 $m^2\ m^{-2}$, the separation point tends to be located at the hill summit (figure not shown), in line with the analytical model in Finnigan and Belcher (2004). Although the hill-induced adverse pressure gradient is dominated by the shape of the hill, it is demonstrated here that an increased LAI leads to enhancement in the adverse pressure

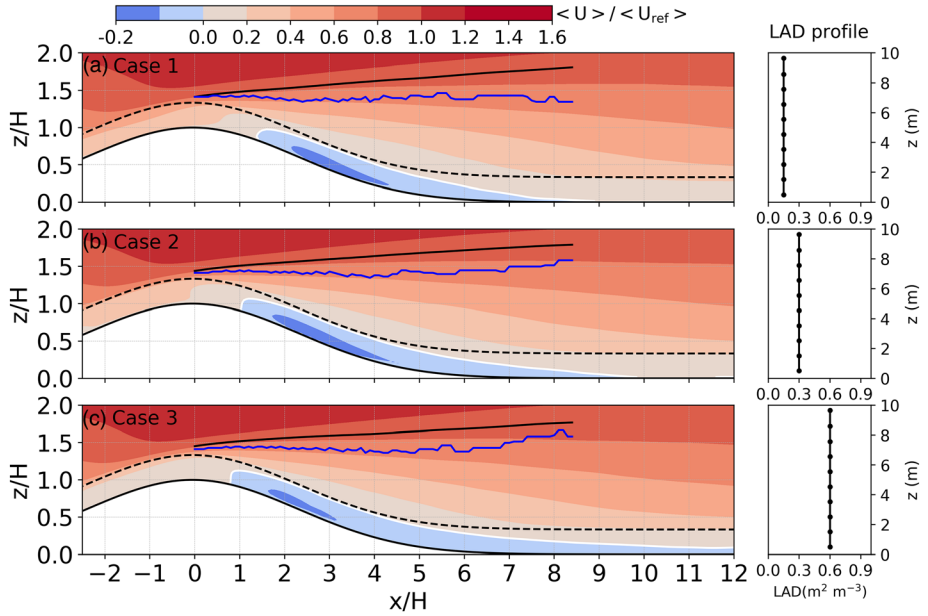

Figure 2. Normalized streamwise velocities for (a) Case 1, (b) Case 2, and (c) Case 3 with different leaf area density. The LAD profiles for these cases are shown in the right panel as references. The white line in the leeward side denotes the region with negative streamwise velocity. The solid black line above denotes depth of the wake region behind the hill. The solid blue line above denotes the shear layer height. The black dashed line denotes the forest top above the hill surface.

gradient and a shift of the minimum pressure center toward the summit (supporting information Figures S1 and S8). The increased LAI causes reduced wind speed within the canopy (less horizontal advection, supporting information Figures S7 and S8) upwind of the separation point, as well as the decreased $\langle u'w' \rangle$ from above into the canopy and the increased canopy drag both upwind and downwind of the separation point. As a consequence, the separation point is shifted toward the summit with increased LAI. In short, the LES here shows nonlinear interaction between the mean pressure (and its longitudinal gradient) and the velocity field (through variations in LAI).

For the flow downwind of the separation point where the recirculation is fully developed, the canopy drag continues to act to decelerate the flow. Since the flow is reversed, this deceleration weakens the recirculating flow. Therefore, an increased LAI is expected to weaken the recirculating flow. This weakening effect is mainly balanced by the pressure gradient force. Note that the maximum depths of the recirculation zones on the leeward region slope for the three cases remain unchanged even though the LAI increases, which is primarily attributed to the dominant adverse pressure gradient and turbulent stress divergence far exceeding the canopy drag over the slope (supporting information Figure S8).

For each of these three cases, the depth of the recirculation decreases rapidly with the increased x/H from the hill foot (i.e., $x/H > 5$). This tendency still emerges in a very dense canopy with LAI = 9 m^2 m^{-2} (result not shown), but the leeward recirculation extends to about $x/H = 20$, though the reverse flow is very weak ($|\langle U \rangle / \langle U_{ref} \rangle| < 0.01$) and restricted to the lower canopy layers (i.e., $z < 0.3\ h$). In addition, the reattachment point is shifted further downwind with increased LAI (Figure 2). The reattachment point is located approximately in the place where the effect of $\langle u'w' \rangle$ and the canopy drag begin to exceed the adverse pressure gradient. In this region, the hill-induced adverse pressure gradient is substantially weakened, and the reverse flow is thus sensitive to changes in amount of $\langle u'w' \rangle$ down into the canopy layer. Therefore, changes in overall LAI have large impacts on the size of the recirculation (i.e., locations of the reattachment point) in this region.

3.1.2. Changes in Velocity Variances and Momentum Flux

Figure 3 shows the profiles of $\frac{\langle U \rangle}{\langle U_{ref} \rangle}$, velocity variances, and $\frac{\langle u'w' \rangle}{\langle U_{ref}{}^2 \rangle}$ for Case 1, Case 2, and Case 3. The above-canopy $\langle U \rangle$ profiles for the three cases are nearly identical at each point across the domain. Within the

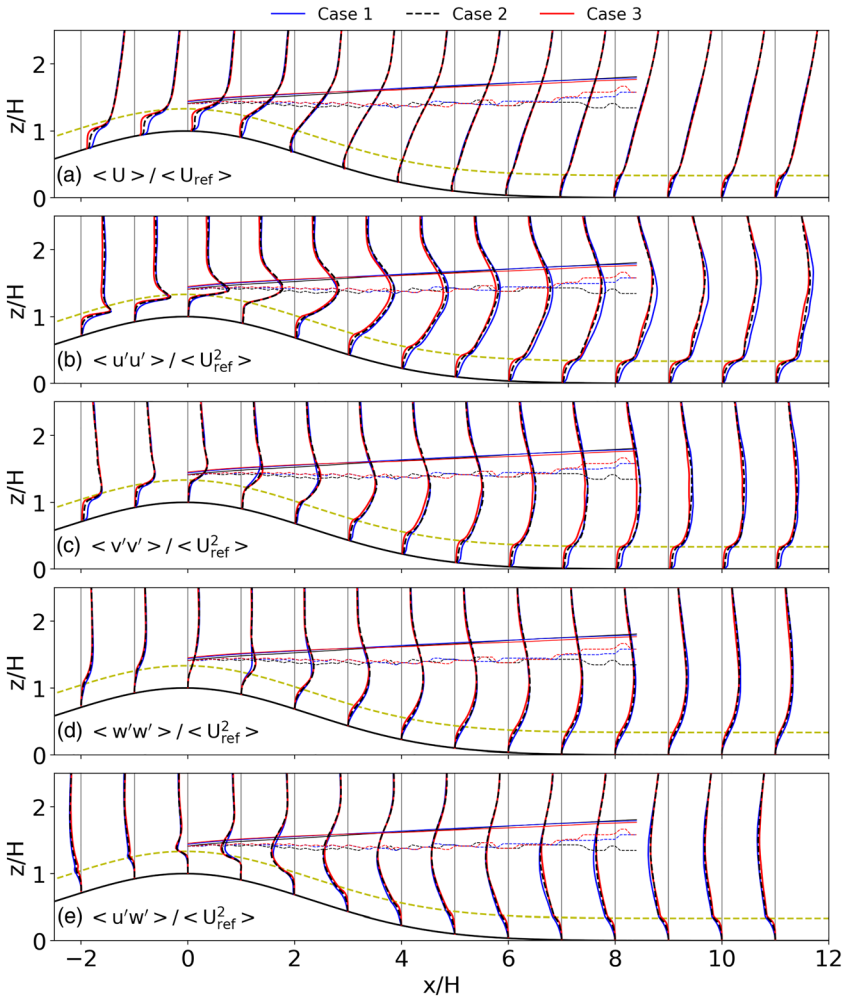

Figure 3. Profiles of the normalized mean and second-order statistics of the flow for Case 1 (blue line), Case 2 (black dashed line), and Case 3 (red line) with uniformly distributed foliage but with different LAI values. The solid lines starting from $x/H = 0$ to $x/H > 8$ denote the wake heights, and the dashed lines denote the shear layer heights for the three cases. The LAI for Case 1 is 1.5 m^2 m^{-2}, the LAI for Case 2 is 3 m^2 m^{-2}, and the LAI for Case 3 is 6 m^2 m^{-2}. Forested region is denoted by yellow dashed lines. (a) The normalized mean streamwise velocity, (b) the normalized streamwise velocity variance, (c) the normalized spanwise velocity variance, (d) the normalized vertical velocity variance, and (e) the normalized momentum flux.

canopy, however, $\langle U \rangle$ decreases with the increased LAI in the region upwind of the separation point ($x/H < 2$) and downwind of the hill foot ($x/H > 7$), with a stronger inflection at the canopy top for the cases with larger LAI, in agreement with prior simulations in Dupont and Brunet (2008). In the region with the recirculating flow, the difference in $\langle U \rangle$ is small but still observable within the canopy in Figure 2.

It was proposed that turbulence in the upper level of the wake region is primarily associated with turbulence structures that originate from the immediate upstream of the summit and are advected and then developed in the wake region (Dupont et al., 2008). The wake depth is defined as the height at which $|\langle U_{lee} \rangle - \langle U_{up} \rangle| / \langle U_{up} \rangle < 0.05$, where $\langle U_{lee} \rangle$ and $\langle U_{up} \rangle$ are the mean streamwise velocity at lee leeward and upstream of the hill, respectively. Under this hypothesis, the leeward flow patterns in the upper level of the wake region are sensitive to the canopy morphology and LAI around the summit. As LAI increases, the canopy roughness around the summit becomes small, thereby leading to the decreased, mechanically generated turbulence that is propagated into the wake region and thus the correspondingly reduced velocity variances in the wake region (Figures 3 and S3–S5). LAI-induced changes in $\langle u'u' \rangle$ occur when $x/$

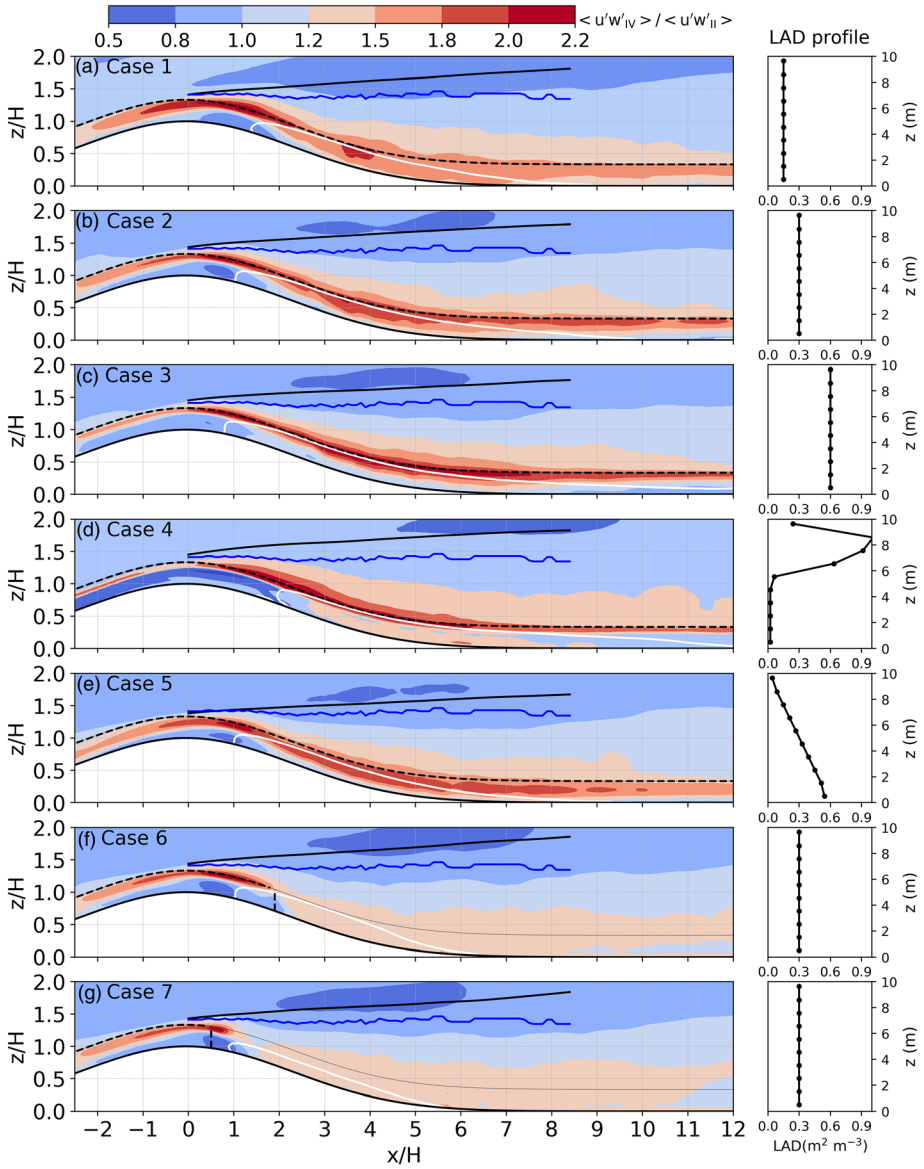

Figure 4. (a–g) Averaged ratios of sweep-induced momentum flux $\langle u'w'_{IV}\rangle$ and ejection-induced momentum flux $\langle u'w'_{II}\rangle$ for all the cases. The white line in the leeward side denotes the region with negative streamwise velocity. The solid black line denotes the depth of the wake region. The solid blue line denotes the shear layer height. The black dashed line denotes the top of the forest canopy. The LAD profiles for these cases are shown in the right panels as references.

$H > 3$ and persist until $x/H = 12$ primarily around the shear layer (the upper part of the wake region where $\langle u'u'\rangle$ becomes the largest), whereas changes in $\langle v'v'\rangle$ and $\langle w'w'\rangle$, which are relatively smaller, occur below the shear layer (the lower part of the wake region) (Figure 3). As LAI increases, however, a reduced $\langle u'w'\rangle$ is observed in the lower part of the wake region, but the difference between the cases is less significant.

It is noticed that the mean upward and downward vertical motions are enhanced upwind and downwind of the summit, respectively, and their centers are also shifted closer to the summit accordingly with increased LAI (supporting information Figure S2). Such changes in $\langle W\rangle$ with increased LAI correspond well to the increased adverse pressure gradient (supporting information Figure S1), which is conjectured to cause the maximum $\langle W\rangle$ to shift toward the summit (Poggi et al., 2008). The aforementioned decreases in the variances and momentum fluxes with increased LAI can be explained by the increased adverse pressure

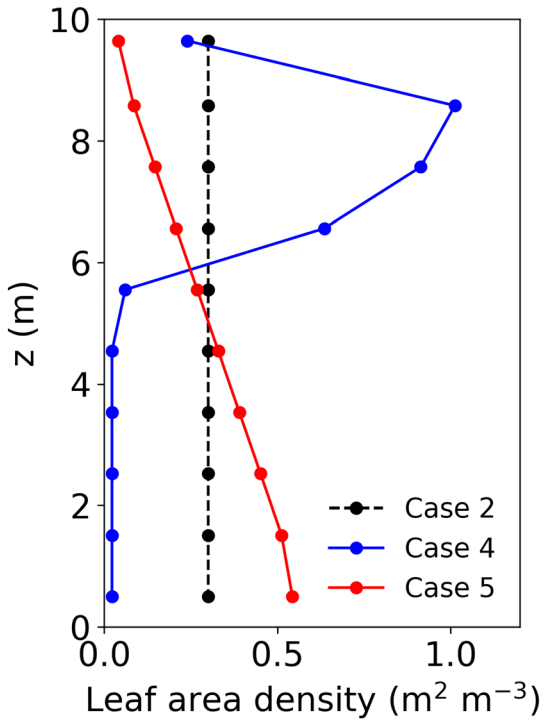

Figure 5. The leaf area density (LAD) profiles for the three cases. The leaf area index (LAI), which is the height-integrated LAD, is identical for the three cases with a value set at 3 m^2 m^{-2}.

gradients that confine turbulence developments and $\langle u'w' \rangle$ on the leeward region, as reflected by the progressively reduced sizes of the leeward maximum variances and $\langle u'w' \rangle$ as well as the position shifts of these maximums toward the summit (supporting information Figures S1–S6). The resulting shifts in these turbulent quantities largely explain the changes in their profiles in Figure 3 (Figure 3 vs. supporting information Figures S3–S6). As LAI increases, the ratio of sweeps $\langle u'w'_{IV} \rangle$ and ejections $\langle u'w'_{II} \rangle$ increases near the canopy top on the leeward region slope (Figure 4), suggesting that the $\langle u'w' \rangle$ contribution from ejections becomes weaker with the increased LAI. Here, sweeps $\langle u'w'_{IV} \rangle$ are the Reynolds stresses in the fourth quadrants, and ejections $\langle u'w'_{II} \rangle$ are the Reynolds stresses in the second quadrants. This feature is also found near the canopy top over flat terrain (Dupont & Brunet, 2008) and largely supported by a wealth of experiments for canopy flows that are sufficiently dense to elicit KH instabilities (Poggi et al., 2004). An explanation that is based on the relative attenuation of $\langle u'u' \rangle$ (weaker) versus $\langle u'w' \rangle$ (stronger) has been offered (Katul et al., 2006) and appears to be compatible with the LES findings here.

3.2. Effects of Canopy Foliage Distributions on the Leeward Flow

3.2.1. Changes in Recirculation

In this section, how nonuniformly distributed foliage regulates the leeward flow and recirculation is now explored. For this purpose, two different foliage distributions are assumed in two additional simulations (Cases 4 and 5), which have the same LAI as Case 2 (Table 1 and Figure 5). Therefore, Case 2 is included here for reference. For Case 4 with a deep trunk space and dense crown layers, the separation point is shifted downwind to $x/H = 2.2$ primarily due to the increased within-canopy horizontal advection (supporting information Figure 8), in line with Banerjee and Linn (2018). The decreased $\langle u'w' \rangle$ from above down into the canopy and the decreased canopy drag in the deep canopy layers have almost identical effects on the force balance upwind and downwind of the separation point. For Case 5 with the high LAD in the lower canopy layers and low LAD in the upper canopy layers, however, the separation point is located at the same position as in Case 2 with a uniformly distributed foliage, although the near-surface LADs differ by a factor of 1.8 between Case 5 and Case 2 (see the LAD profiles in Figure 5). As compared with Case 2, the mild increase in adverse pressure gradient in Case 5 is mainly balanced by the increase in canopy drag (supporting information Figure S8), leading to the unchanged positions of the separation points for these two cases. Over the leeward region slopes, due to the smaller turbulence stress divergence near the canopy top as compared with that in Case 5, the maximum depth of the recirculating flows is slightly larger in Case 4. Deep within the canopy, an enhanced reverse flow is evident in Case 4 ($|\langle U \rangle / \langle U_{ref} \rangle| = 0.25$) in the leeward of $3 < x/H < 6$, as compared with Case 5 ($|\langle U \rangle / \langle U_{ref} \rangle| = 0.1$) (Figures 6 and 7).

The reattachment point is shifted further downwind for Case 4 ($x/H = 12$), compared to Case 2 ($x/H = 9.8$). This result is consistent with the analysis in section 3.1 that the stronger adverse pressure gradient, stronger upper canopy absorption of turbulence (i.e., less $\langle u'w' \rangle$ into the canopy leading to small turbulent stress gradients), and weaker drag force in the lower canopy layers are responsible for developing a longer recirculation (supporting information Figure S8). The reattachment point in Case 5 ($x/H = 9.2$) is largely shifted upwind, as compared with Case 2 and Case 4, which is primarily attributed to the increased $\langle u'w' \rangle$ into the canopy layer.

3.2.2. Changes in Velocity Variances and Momentum Flux

Due to the small canopy drag in the lower canopy layers, the accelerated winds (i.e., the secondary maximum $\langle U \rangle / \langle U_{ref} \rangle$) upwind of the summit in Case 4 also generate the evident secondary maximum in $\langle u'u' \rangle$ and $\langle v'v' \rangle$, indicating the highly turbulent flow in this region (Figure 7). This secondary maximum $\langle U \rangle / \langle U_{ref} \rangle$ within the canopy causes positive momentum flux into the upper canopy layers (Figure 7e). However, this secondary maximum is absent in a uniformly distributed forest where

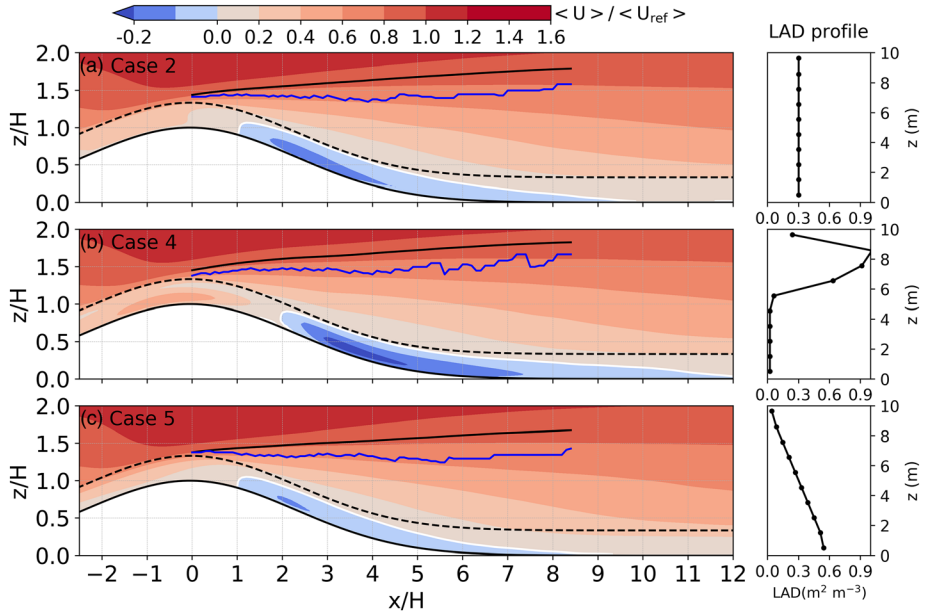

Figure 6. Normalized streamwise velocities for (b) Case 4 and (c) Case 5 with the different foliage distributions. Case 2 in panel (a) is also shown as reference. The white line in the leeward side denotes the region with negative streamwise velocity. The solid black line denotes the depth of the wake region behind the hill. The solid blue line denotes the shear layer height. The black dashed line denotes the forest above the hill. The LAD profiles for these cases are shown in the right panel as references.

turbulence is small, and the advection is usually negligible (Finnigan & Belcher, 2004; Katul, Finnigan, et al., 2006).

The $\langle U \rangle$ in the wake region above the canopy shows noticeable differences between the two cases with the same LAI value suggesting the influence of vertical foliage distributions on mean flow (Figure 7a). The denser crown canopy layer causes the larger velocity inflection and the stronger shear layer to be elevated to higher levels in Case 4 in the upwind of the summit region ($-2 < x/H < 0$), which initiates turbulent eddies to be propagated in the upper level of the wake region, leading to a reduction in $\langle U \rangle$ and thus the corresponding upward shifts in the variance maxima (Figure 7). As a result, the three variances for Case 4 are greater (smaller) than those for Case 5 in the upper (lower) level of the wake region. Such increased heights for the variance maximums in Case 4 correspond to the higher inflection point in $\langle U \rangle$ at $x/H = -1$, where the leeward turbulence originates. A similar feature is also observed for $\langle u'w' \rangle$ (Figure 7e). As the foliage becomes denser in the upper canopy layers, sweeping eddies seem to be difficult to penetrate into the deeper layers of the canopy, showing a smaller ratio of sweeps and ejections within the canopy (Figures 4d and 4e) and a reduced $\langle u'w' \rangle$ within the canopy for Case 4.

Although the three cases have the same LAI, there is a progressively increased adverse pressure gradient from Case 4 to Case 2 and to Case 5, suggesting the influence of the varying vertical foliage distribution on the hill-induced adverse pressure gradients (supporting information Figure S1). Such gradually increased adverse pressure gradients make the minimum pressure zones and the corresponding $\langle w'w' \rangle$ zones to shift toward the summit, which causes the progressively enlarged mean vertical velocity zones and the corresponding increased $\langle w'w' \rangle$ zones from Case 4 to Case 2 and to Case 5 (supporting information Figure S2). Additionally, the gradually increased adverse pressure gradients suppress the variances and push their maximum zones to shift toward the summit (supporting information Figures S3–S6). Such changes in their patterns also largely explain their corresponding profiles in Figure 7.

3.3. Effects of Forest Edge on the Leeward Flows

By partially replacing forest with bare soil characterized by a roughness length of 0.1 m on the leeward region slope to create a forest edge, the role of a leeward forest in regulating the mean flow and turbulence can be explored. The inflow conditions near the canopy top are identical for all the cases such that the

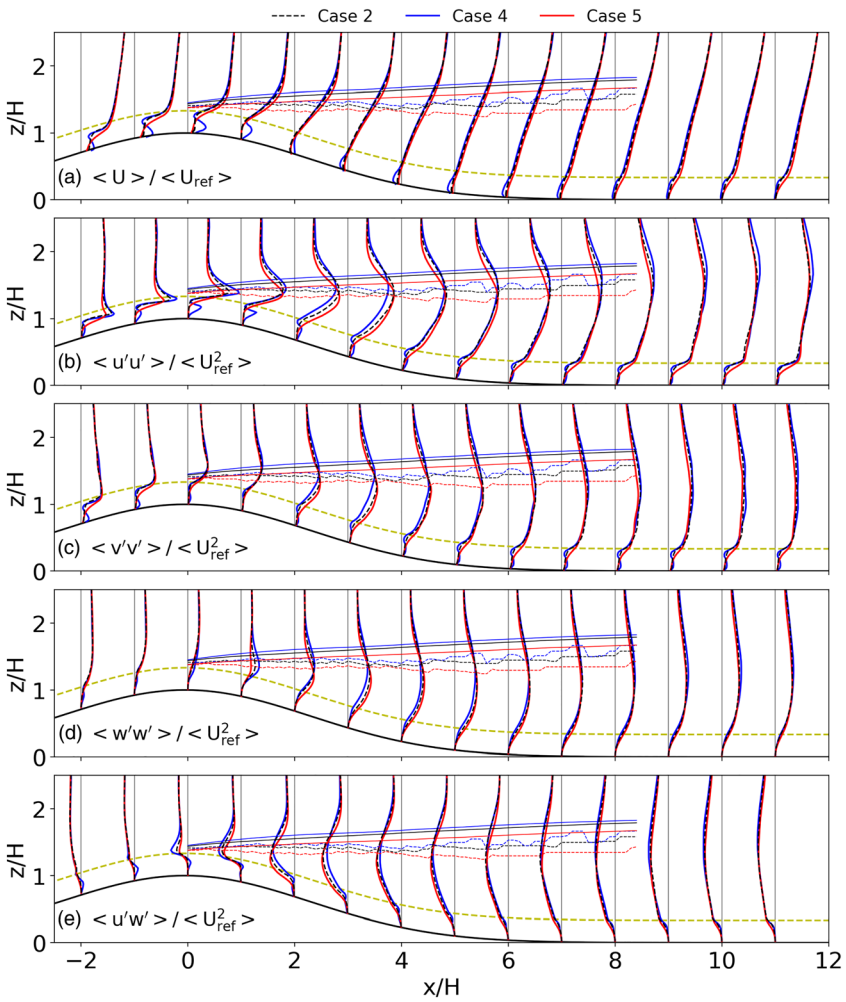

Figure 7. Vertical profiles of the normalized mean and second-order statistics of the flow for Case 4 (blue line) and Case 5 (red line) with two different foliage distributions. Note that Case 2 is also shown for comparison. The solid lines starting $x/H = 0$ to $x/H > 8$ above the leeward slope denote the wake heights, and the dashed lines denote the shear layer heights for the three cases. Forested region is denoted by yellow dashed lines. (a) The normalized mean streamwise velocity, (b) the normalized streamwise velocity variance, (c) the normalized spanwise velocity variance, (d) the normalized vertical velocity variance, and (e) the normalized momentum flux.

influence of canopy removal can be compared directly. Two cases are implemented: Cases 6 and 7 where the canopy in Case 2 is partially removed in the different regions of the leeward region slope (i.e., the forested region in $x/H < 1.9$ for Case 6 and $x/H < 0.5$ for Case 7 in Table 1).

3.3.1. Changes in Recirculation

Figure 8 shows the contours of the normalized streamwise component of the mean velocity for Cases 6 and 7. Case 2 is used for comparison. One notable difference is the changes in the recirculation for Case 6 and Case 7 as compared with Case 2. As for Case 2 with a fully forested hill, the recirculation zone starts at $x/H = 1.0$ (the separation point) and ends at $x/H = 9.8$ (the reattachment point). In Case 6 with the canopy removal (i.e., the canopy ends at $x/H = 1.9$), the separation point remains the same (i.e., $x/H = 1.0$) and the reattachment point is largely shifted toward the summit (i.e., $x/H = 6.3$) compared with Case 2 (i.e., $x/H = 9.8$). The maximum depth of the recirculation remains unchanged. In Case 7 with further canopy removal (i.e., the canopy ends at $x/H = 0.5$), the longitudinal extension of the recirculation is largely reduced with its separation ending at $x/H = 0.9$ and the reattachment point at $x/H = 5.7$, and its maximum depth is decreased to about half of that for both Case 2 and Case 6.

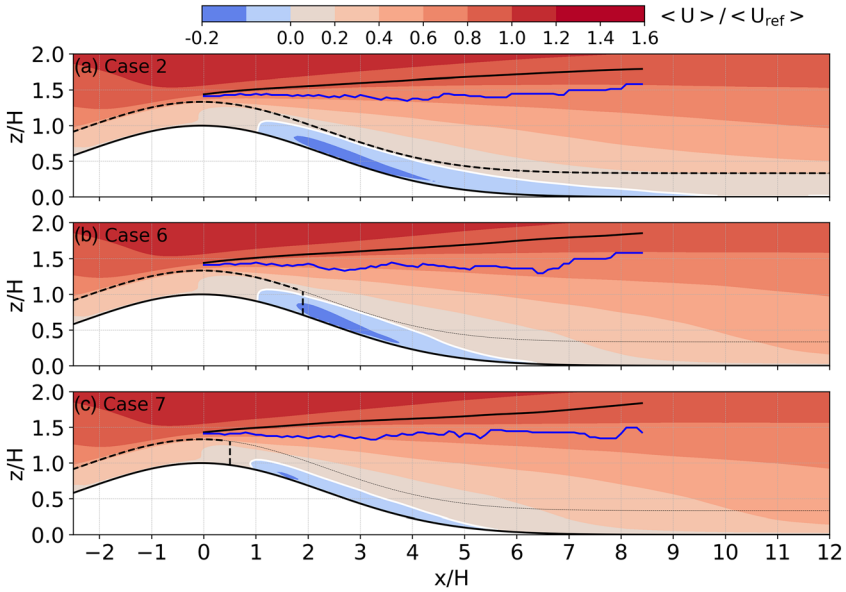

Figure 8. Normalized streamwise velocities for (b) Case 6 and (c) Case 7 with different forest coverage regions. Case 2 in panel (a) is also shown as reference. The black dashed line denotes the forest above the hill. The white line in the leeward side denotes the region with negative streamwise velocity. The solid black line above denotes depth of the wake region behind the hill. The solid blue line above denotes the shear layer height.

For Case 6, the separation point is still located in the forested region, which means that all the forces that determine the separation point position in Case 2 remain unchanged in Case 6 (supporting information Figures S7 and S8), leading to the unchanged position of the separation point. In addition, the effect of the canopy removal on the recirculation is primarily in the downstream of the edge ($x/H > 1.9$), and the edge effect is localized. For Case 7, however, further canopy removal to the upstream of the separation point largely alters the force balance around the separation point. The slight shift of the separation point toward the summit in Case 7 is primarily attributed to forest edge effect, which induces the balance mainly between the increased negative turbulence stress divergence and the slightly increased pressure gradient (supporting information Figure S7) (Banerjee et al., 2013).

Without the canopy to weaken $\langle u'w' \rangle$ from above, the near-surface turbulence and $\langle u'w' \rangle$ become greater at $x/H = 2$ and increase with the increasing x/H in Case 6 and Case 7 than Case 2 (Figure 9e; supporting information Figures S3–S6). Such stronger downward $\langle u'w' \rangle$ and enhanced turbulence (i.e., larger negative turbulence stress divergences) suppress the maximum depths of the recirculating flows, as reflected by the much lower recirculation depth for Case 7 (Figure 8). In addition, the reattachment points are shifted largely toward the summit due to the increased $\langle u'w' \rangle$ leading to large turbulent stress gradients far exceeding the adverse pressure gradient.

3.3.2. Changes in Velocity Variances and Momentum Flux

Turbulence in the upper level of the wake region is primarily associated with turbulence structures generated in the proximity upstream of the summit and thus are subjected to the influence of the canopy morphology there. The identical LAI and vertical foliage distributions in the proximity of the summit in Case 2, Case 6, and Case 7 indicate that the turbulence sources for the three cases are also identical. Therefore, the differences in turbulence structures in the upper level of the wake region among the three cases predominantly result from edge-induced changes in the hill-induced adverse pressure gradients, given the fact that the direct impacts from the edge on turbulence are localized. From the fully forested hill (Case 2) to the partial canopy removal in Case 6 and Case 7, the adverse pressure gradients are enhanced on the leeward (supporting information Figure S1), leading to a shift of the mean velocity streamlines toward the summit (i.e., $\langle U \rangle$ in Figures 8 and 1b and $\langle W \rangle$ in supporting information Figure S2). Correspondingly, the enhanced adverse pressure gradients also suppress turbulence developments and momentum flux transfer and cause a corresponding shift of their maximum zones toward the summit (supporting information Figures S3–S6), which

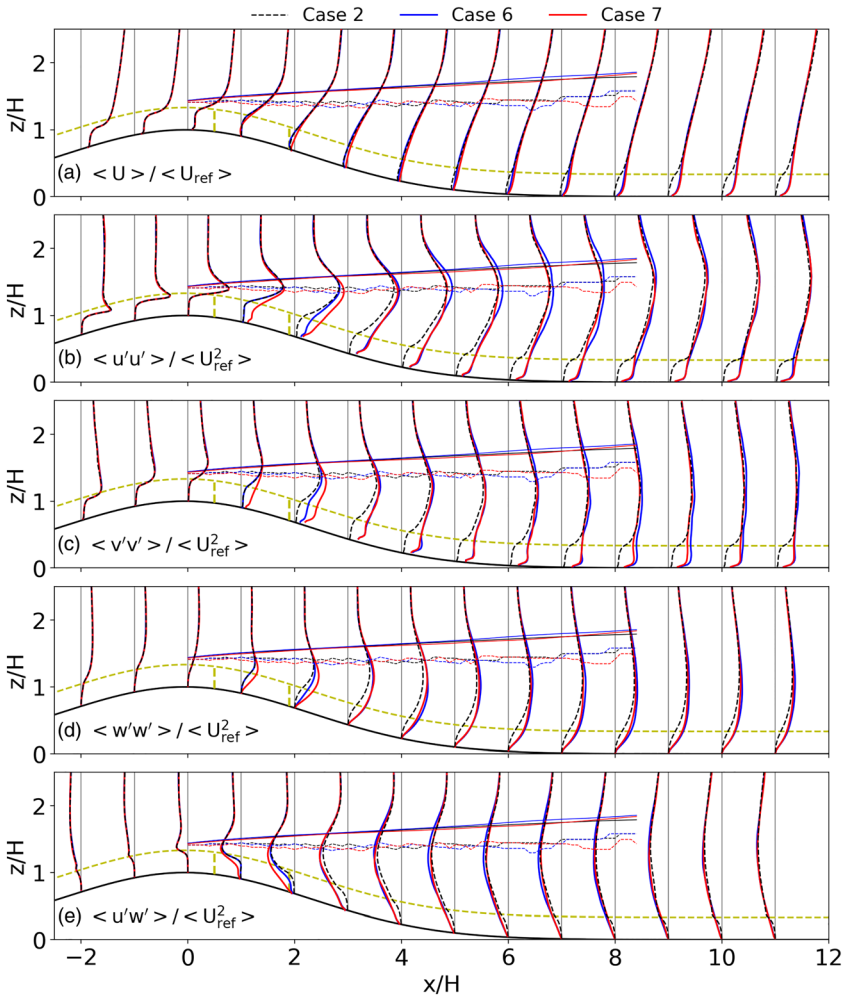

Figure 9. Vertical profiles of the normalized mean and second-order statistics of the flow for Case 6 (blue line) and Case 7 (red line) with different forest coverage regions. Note that Case 2 is also shown for comparison. The solid lines starting from $x/H = 0$ to $x/H > 8$ above the leeward slope denotes the wake heights, and the dashed lines denote the shear layer heights. Forested region is denoted by yellow dashed lines. (a) The normalized mean streamwise velocity, (b) the normalized streamwise velocity variance, (c) the normalized spanwise velocity variance, (d) the normalized vertical velocity variance, and (e) the normalized momentum flux.

are the primary reasons for the changes in their profiles in Figure 9. As a result, the partial canopy removals in Cases 6 and 7 cause the increased variances and momentum from the surface up to the upper level of the wake region, but such an increase is more pronounced near the surface and in the lower levels of the wake region, as compared with Case 2. Note that the edge-induced changes in the three variances and momentum persist only over a short distance from the edge and a short vertical extension. Turbulence near the surface, or more precisely, in the inner layer ($z < h_i$) is in a local equilibrium (Hunt et al., 1988), where the mean advection is small and the fluctuations are mainly determined by local conditions. The fraction of sweeps $\langle u'w'_{IV}\rangle$ and ejections $\langle u'w'_{II}\rangle$ on the leeward indicates that sweeps continue to dominate over ejections in momentum transfer in the lower level of the wake region, whereas ejections play dominant roles in momentum transfer in the upper level (Figure 4).

4. Conclusions

The LES results over a forested hill with varying leaf area densities, vertical foliage distribution, and forest coverage regions unpack the effect of canopy morphology on leeward flows. Although the pressure perturbation is dominated by the shape of the hill, it is demonstrated here that changes in canopy morphology

modulate intensities and patterns of the leeward adverse pressure gradients and their positions. That is, the vegetation-hill pressure-velocity system is interactive despite the mild slope imposed. A recirculation zone identified by regions of negative mean longitudinal velocity develops in all the cases, but changes are found in its position as well as its strengths and depths. Turbulence structures generated around the summit are dependent upon canopy morphology there, which are then advected downwind into the wake regions. However, mean flow fields and turbulence developments in the wake region are largely modulated by the adverse pressure gradients, leading to changes in the patterns and locations of the strong mean vertical velocity zones. The forest edge effects on leeward flow can be significant and act through modulating the hill-induced adverse pressure gradients, but the direct influence of the edge on the flows remains localized. Since the simultaneous effects of the hill and canopy morphologies on the leeward flow dynamics and fluxes occur well above the wake zone, any flux measurements over such complex settings should be conducted above this zone. It should also be noted that neutral canopy flows over hills are the focus here; therefore, how stable and unstable stratifications modulate canopy flow dynamics observed here are better kept for future inquiries.

Data Availability Statement

Data generated by the model for all figures can be accessed through figshare (https://figshare.com/articles/dataset/The_effects_of_canopy_morphology_on_flow_over_a_two-dimensional_isolated_ridge/12782435).

Acknowledgments
We thank Qi Li and an anonymous reviewer for their constructive comments that improved the quality of our manuscript. Y. Ma and H. Liu acknowledge support from the U.S. National Science Foundation (NSF) under Grants NSF-AGS-1419614 and NSF-AGS-1853050; G. Katul acknowledges support from NSF under Grants NSF-AGS-1644382, NSF-AGS-2028633, and NSF-IOS-1754893. The high-performance computing support from Cheyenne (doi:10.5065/D6RX99HX) provided by NCAR's Computational and Information Systems Laboratory, sponsored by NSF, is also acknowledged.

References

Allen, T. (2006). Flow over hills with variable roughness. *Boundary-Layer Meteorology*, *121*(3), 475–490. https://doi.org/10.1007/s10546-006-9086-0

Banerjee, T., Katul, G., Fontan, S., Poggi, D., & Kumar, M. (2013). Mean flow near edges and within cavities situated inside dense canopies. *Boundary-Layer Meteorology*, *149*(1), 19–41. https://doi.org/10.1007/s10546-013-9826-x

Banerjee, T., & Linn, R. (2018). Effect of vertical canopy architecture on transpiration, thermoregulation and carbon assimilation. *Forests*, *9*(4), 198. https://doi.org/10.3390/f9040198

Belcher, S. E., Finnigan, J. J., & Harman, I. N. (2008). Flows through forest canopies in complex terrain. *Ecological Applications*, *18*(6), 1436–1453. https://doi.org/10.1890/06-1894.1

Belcher, S. E., Harman, I. N., & Finnigan, J. J. (2012). The wind in the willows: Flows in forest canopies in complex terrain. *Annual Review of Fluid Mechanics*, *44*(1), 479–504. https://doi.org/10.1146/annurev-fluid-120710-101036

Belcher, S. E., & Hunt, J. C. R. (1998). Turbulent flow over hills and waves. *Annual Review of Fluid Mechanics*, *30*(1), 507–538. https://doi.org/10.1146/annurev.fluid.30.1.507

Bitsuamlak, G. T., Stathopoulos, T., & Bédard, C. (2004). Numerical evaluation of wind flow over complex terrain. *Journal of Aerospace Engineering*, *17*(4), 135–145. https://doi.org/10.1061/(ASCE)0893-1321(2004)17:4(135)

Bou-Zeid, E., Meneveau, C., & Parlange, M. (2005). A scale-dependent Lagrangian dynamic model for large eddy simulation of complex turbulent flows. *Physics of Fluids*, *17*(2), 025105. https://doi.org/10.1063/1.1839152

Cao, S., Wang, T., Ge, Y., & Tamura, Y. (2012). Numerical study on turbulent boundary layers over two-dimensional hills—Effects of surface roughness and slope. *Journal of Wind Engineering and Industrial Aerodynamics*, *104*, 342–349.

Cassiani, M., Katul, G. G., & Albertson, J. D. (2008). The effects of canopy leaf area index on airflow across forest edges: Large-eddy simulation and analytical results. *Boundary-Layer Meteorology*, *126*(3), 433–460. https://doi.org/10.1007/s10546-007-9242-1

Chen, B., Chamecki, M., & Katul, G. G. (2019). Effects of topography on in-canopy transport of gases emitted within dense forests. *Quarterly Journal of the Royal Meteorological Society*, *145*(722), 2101–2114. https://doi.org/10.1002/qj.3546

Chen, H., & Yi, C. (2012). Optimal control of katabatic flows within canopies. *Quarterly Journal of the Royal Meteorological Society*, *138*(667), 1676–1680. https://doi.org/10.1002/qj.1904

Dupont, S., & Brunet, Y. (2008). Influence of foliar density profile on canopy flow: A large-eddy simulation study. *Agricultural and Forest Meteorology*, *148*(6–7), 976–990. https://doi.org/10.1016/j.agrformet.2008.01.014

Dupont, S., Brunet, Y., & Finnigan, J. J. (2008). Large-eddy simulation of turbulent flow over a forested hill: Validation and coherent structure identification. *Quarterly Journal of the Royal Meteorological Society*, *134*(636), 1911–1929. https://doi.org/10.1002/qj.328

Finnigan, J., Harman, I., Ross, A., & Belcher, S. (2015). First-order turbulence closure for modelling complex canopy flows. *Quarterly Journal of the Royal Meteorological Society*, *141*(692), 2907–2916. https://doi.org/10.1002/qj.2577

Finnigan, J. J., & Belcher, S. E. (2004). Flow over a hill covered with a plant canopy. *Quarterly Journal of the Royal Meteorological Society*, *130*(596), 1–29. https://doi.org/10.1256/qj.02.177

Finnigan, J. J., & Brunet, Y. (1995). Turbulent airflow in forests on flat and hilly terrain. In M. P. Coutts, & J. Grace (Eds.), *Wind and trees* (pp. 3–40). Cambridge, UK: Cambridge University press.

Fontan, S., Katul, G. G., Poggi, D., Manes, C., & Ridolfi, L. (2013). Flume experiments on turbulent flows across gaps of permeable and impermeable boundaries. *Boundary-Layer Meteorology*, *147*(1), 21–39. https://doi.org/10.1007/s10546-012-9772-z

Grant, E. R., Ross, A. N., & Gardiner, B. A. (2016). Modelling canopy flows over complex terrain. *Boundary-Layer Meteorology*, *161*(3), 417–437. https://doi.org/10.1007/s10546-016-0176-3

Harman, I. N., & Finnigan, J. J. (2010). Flow over hills covered by a plant canopy: Extension to generalised two-dimensional topography. *Boundary-Layer Meteorology*, *135*(1), 51–65. https://doi.org/10.1007/s10546-009-9458-3

Hunt, J. C. R., Leibovich, S., & Richards, K. J. (1988). Turbulent shear flows over low hills. *Quarterly Journal of the Royal Meteorological Society*, *114*(484), 1435–1470. https://doi.org/10.1002/qj.49711448405

Juang, J. Y., Katul, G. G., Siqueira, M. B., Stoy, P. C., & McCarthy, H. R. (2008). Investigating a hierarchy of Eulerian closure models for scalar transfer inside forested canopies. *Boundary-Layer Meteorology*, *128*(1), 1–32. https://doi.org/10.1007/s10546-008-9273-2

Kader, B. A., & Yaglom, A. M. (1978). Similarity treatment of moving-equilibrium turbulent boundary layers in adverse pressure gradients. *Journal of Fluid Mechanics*, *89*(2), 305–342. https://doi.org/10.1017/S0022112078002621

Katul, G. G., & Chang, W. H. (1999). Principal length scales in second-order closure models for canopy turbulence. *Journal of Applied Meteorology*, *38*(11), 1631–1643. https://doi.org/10.1175/1520-0450(1999)038<1631:PLSISO>2.0.CO;2

Katul, G. G., Finnigan, J. J., Poggi, D., Leuning, R., & Belcher, S. E. (2006). The influence of hilly terrain on canopy-atmosphere carbon dioxide exchange. *Boundary-Layer Meteorology*, *118*(1), 189–216. https://doi.org/10.1007/s10546-005-6436-2

Katul, G. G., Mahrt, L., Poggi, D., & Sanz, C. (2004). One-and two-equation models for canopy turbulence. *Boundary-Layer Meteorology*, *113*(1), 81–109. https://doi.org/10.1023/B:BOUN.0000037333.48760.e5

Katul, G. G., & Poggi, D. (2010). The influence of hilly terrain on aerosol-sized particle deposition into forested canopies. *Boundary-Layer Meteorology*, *135*(1), 67–88. https://doi.org/10.1007/s10546-009-9459-2

Katul, G. G., Poggi, D., Cava, D., & Finnigan, J. (2006). The relative importance of ejections and sweeps to momentum transfer in the atmospheric boundary layer. *Boundary-Layer Meteorology*, *120*(3), 367–375.

Kobayashi, M. H., Pereira, J. C. F., & Siqueira, M. B. B. (1994). Numerical study of the turbulent flow over and in a model forest on a 2D hill. *Journal of Wind Engineering and Industrial Aerodynamics*, *53*(3), 357–374. https://doi.org/10.1016/0167-6105(94)90091-4

Kröniger, K., Banerjee, T., De Roo, F., & Mauder, M. (2018). Flow adjustment inside homogeneous canopies after a leading edge—An analytical approach backed by LES. *Agricultural and Forest Meteorology*, *255*, 17–30. https://doi.org/10.1016/j.agrformet.2017.09.019

Kutter, E., Yi, C., Hendrey, G., Liu, H., Eaton, T., & Ni-Meister, W. (2017). Recirculation over complex terrain. *Journal of Geophysical Research: Atmospheres*, *122*, 6637–6651. https://doi.org/10.1002/2016JD026409

Lin, X., Chamecki, M., Katul, G., & Yu, X. (2018). Effects of leaf area index and density on ultrafine particle deposition onto forest canopies: A LES study. *Atmospheric Environment*, *189*, 153–163. https://doi.org/10.1016/j.atmosenv.2018.06.048

Liu, Z., Cao, S., Liu, H., & Ishihara, T. (2019). Large-eddy simulations of the flow over an isolated three-dimensional hill. *Boundary-Layer Meteorology*, *170*(3), 415–441. https://doi.org/10.1007/s10546-018-0410-2

Liu, Z., Ishihara, T., Tanaka, T., & He, X. (2016). LES study of turbulent flow fields over a smooth 3-D hill and a smooth 2-D ridge. *Journal of Wind Engineering and Industrial Aerodynamics*, *153*, 1–12. https://doi.org/10.1016/j.jweia.2016.03.001

Ma, Y., & Liu, H. (2017). Large-eddy simulations of atmospheric flows over complex terrain using the immersed-boundary method in the Weather Research and Forecasting Model. *Boundary-Layer Meteorology*, *165*(3), 421–445. https://doi.org/10.1007/s10546-017-0283-9

Ma, Y., & Liu, H. (2019). An advanced multiple-layer canopy model in the WRF model with large-eddy simulations to simulate canopy flows and scalar transport under different stability conditions. *Journal of Advances in Modeling Earth Systems*, *11*(7), 2330–2351. https://doi.org/10.1029/2018MS001347

Ma, Y., Liu, H., Liu, Z., Yi, C., & Lamb, B. (2020). Influence of forest-edge flows on scalar transport with different vertical distributions of foliage and scalar sources. *Boundary-Layer Meteorology*, *174*(1), 99–117.

Massman, W. J. (1997). An analytical one-dimensional model of momentum transfer by vegetation of arbitrary structure. *Boundary-Layer Meteorology*, *83*(3), 407–421. https://doi.org/10.1023/A:1000234813011

Meyers, T. (1986). Testing of a higher-order closure model for modeling airflow within and above plant canopies. *Boundary-Layer Meteorology*, *37*(3), 297–311. https://doi.org/10.1007/BF00122991

Morse, A. P., Gardiner, B. A., & Marshall, B. J. (2002). Mechanisms controlling turbulence development across a forest edge. *Boundary-Layer Meteorology*, *103*(2), 227–251. https://doi.org/10.1023/A:1014507727784

Patton, E. G., & Katul, G. G. (2009). Turbulent pressure and velocity perturbations induced by gentle hills covered with sparse and dense canopies. *Boundary-Layer Meteorology*, *133*(2), 189–217. https://doi.org/10.1007/s10546-009-9427-x

Pearse, J. R., Lindley, D., & Stevenson, D. C. (1981). Wind flow over ridges in simulated atmospheric boundary layers. *Boundary-Layer Meteorology*, *21*(1), 77–92. https://doi.org/10.1007/BF00119369

Poggi, D., & Katul, G. (2007a). The ejection-sweep cycle over bare and forested gentle hills: A laboratory experiment. *Boundary-Layer Meteorology*, *122*(3), 493–515. https://doi.org/10.1007/s10546-006-9117-x

Poggi, D., & Katul, G. G. (2007b). An experimental investigation of the mean momentum budget inside dense canopies on narrow gentle hilly terrain. *Agricultural and Forest Meteorology*, *144*(1–2), 1–13. https://doi.org/10.1016/j.agrformet.2007.01.009

Poggi, D., & Katul, G. G. (2007c). Turbulent flows on forested hilly terrain: The recirculation region. *Quarterly Journal of the Royal Meteorological Society*, *133*(625), 1027–1039. https://doi.org/10.1002/qj.73

Poggi, D., & Katul, G. G. (2008). Turbulent intensities and velocity spectra for bare and forested gentle hills: Flume experiments. *Boundary-Layer Meteorology*, *129*(1), 25–46. https://doi.org/10.1007/s10546-008-9308-8

Poggi, D., Katul, G. G., Finnigan, J. J., & Belcher, S. E. (2008). Analytical models for the mean flow inside dense canopies on gentle hilly terrain. *Quarterly Journal of the Royal Meteorological Society*, *134*(634), 1095–1112. https://doi.org/10.1002/qj.276

Poggi, D., Porporato, A., Ridolfi, L., Albertson, J. D., & Katul, G. G. (2004). The effect of vegetation density on canopy sub-layer turbulence. *Boundary-Layer Meteorology*, *111*(3), 565–587. https://doi.org/10.1023/B:BOUN.0000016576.05621.73

Ross, A. N. (2008). Large-eddy simulations of flow over forested ridges. *Boundary-Layer Meteorology*, *128*(1), 59–76. https://doi.org/10.1007/s10546-008-9278-x

Ross, A. N. (2011). Scalar transport over forested hills. *Boundary-Layer Meteorology*, *141*(2), 179–199. https://doi.org/10.1007/s10546-011-9628-y

Ross, A. N., & Baker, T. P. (2013). Flow over partially forested ridges. *Boundary-Layer Meteorology*, *146*(3), 375–392. https://doi.org/10.1007/s10546-012-9766-x

Ross, A. N., & Vosper, S. B. (2005). Neutral turbulent flow over forested hills. *Quarterly Journal of the Royal Meteorological Society*, *131*(609), 1841–1862. https://doi.org/10.1256/qj.04.129

Simpson, C. C., Sharples, J. J., Evans, J. P., & McCabe, M. F. (2013). Large eddy simulation of atypical wildland fire spread on leeward slopes. *International Journal of Wildland Fire*, *22*(5), 599–614. https://doi.org/10.1071/WF12072

Shaw, R. H., & Patton, E. G. (2003). Canopy element influences on resolved-and subgrid-scale energy within a large-eddy simulation. *Agricultural and Forest Meteorology*, *115*(1–2), 5–17. https://doi.org/10.1016/S0168-1923(02)00165-X

Skamarock, W.C., Klemp, J. B., Dudhia, J., Gill, D. O., Barker, D. M., Duda, M. G., et al. (2008). A description of the advanced research WRF version 3. NCAR technical notes, NCAR/TN-4751STR.

Wang, W., & Yi, C. (2012). A new nonlinear analytical model for canopy flow over a forested hill. *Theoretical and Applied Climatology*, *109*(3–4), 549–563. https://doi.org/10.1007/s00704-012-0599-9

Wang, W. J., Peng, W. Q., Huai, W. X., Katul, G. G., Liu, X. B., Qu, X. D., & Dong, F. (2019). Friction factor for turbulent open channel flow covered by vegetation. *Scientific Reports*, *9*(1), 1–16.

Wilson, J. D. (1988). A second-order closure model for flow through vegetation. *Boundary-Layer Meteorology*, *42*(4), 371–392. https://doi.org/10.1007/BF00121591

Wilson, J. D., Finnigan, J. J., & Raupach, M. R. (1998). A first-order closure for diturbed plant-canopy flows, and its application to winds in a canopy on a ridge. *Quarterly Journal of the Royal Meteorological Society*, *124*(547), 705–732.

Wilson, N. R., & Shaw, R. H. (1977). A higher order closure model for canopy flow. *Journal of Applied Meteorology*, *16*(11), 1197–1205. https://doi.org/10.1175/1520-0450(1977)016<1197:AHOCMF>2.0.CO;2

Xu, X., & Yi, C. (2013). The influence of geometry on recirculation and CO_2 transport over forested hills. *Meteorology and Atmospheric Physics*, *119*(3–4), 187–196. https://doi.org/10.1007/s00703-012-0224-6

Yaglom, A. M. (1979). Similarity laws for constant-pressure and pressure-gradient turbulent wall flows. *Annual Review of Fluid Mechanics*, *11*(1), 505–540. https://doi.org/10.1146/annurev.fl.11.010179.002445

Yang, X., Howard, K. B., Guala, M., & Sotiropoulos, F. (2015). Effects of a three-dimensional hill on the wake characteristics of a model wind turbine. *Physics of Fluids*, *27*(2), 025103. https://doi.org/10.1063/1.4907685

Yi, C. (2008). Momentum transfer within canopies. *Journal of Applied Meteorology and Climatology*, *47*(1), 262–275. https://doi.org/10.1175/2007JAMC1667.1

Zitouna-Chebbi, R., Prévot, L., Jacob, F., & Voltz, M. (2015). Accounting for vegetation height and wind direction to correct eddy covariance measurements of energy fluxes over hilly crop fields. *Journal of Geophysical Research: Atmospheres*, *120*, 4920–4936. https://doi.org/10.1002/2014JD022999